PLOS ONE

RESEARCH ARTICLE

Bile acids target proteolipid nano-assemblies of EGFR and phosphatidic acid in the plasma membrane for stimulation of MAPK signaling

Hong Liang[1], Mary K. Estes[2], Huiling Zhang[3], Guangwei Du[1], Yong Zhou[1]*

1 Department of Integrative Biology and Pharmacology, University of Texas Health Science Center, Houston, Texas, United States of America, **2** Department of Molecular Virology and Microbiology, Baylor College of Medicine, Houston, Texas, United States of America, **3** College of Pharmaceutical Sciences, Soochow University, Suzhou, P.R. China

* yong.zhou@uth.tmc.edu

Citation: Liang H, Estes MK, Zhang H, Du G, Zhou Y (2018) Bile acids target proteolipid nano-assemblies of EGFR and phosphatidic acid in the plasma membrane for stimulation of MAPK signaling. PLoS ONE 13(8): e0198983. https://doi.org/10.1371/journal.pone.0198983

Editor: Sheereen Majd, University of Houston, UNITED STATES

Received: May 25, 2018

Accepted: August 17, 2018

Published: August 31, 2018

Data Availability Statement: All relevant data are within the paper and its Supporting Information files.

Funding: This work was supported by The National Institute of Diabetes and Digestive and Kidney Diseases grant no. DK056338 to MKE and YZ, The National Institute of Aging grant no. AI57788 to MKE, and The National Institute of Heart, Lung and Blood Institute grant no. HL119478 to GD. The funders had no role in study design, data collection

Abstract

Bile acids are critical biological detergents in the gastrointestinal tract and also act as messengers to regulate a multitude of intracellular signaling events, including mitogenic signaling, lipid metabolism and endo/exocytosis. In particular, bile acids stimulate many receptors and ion channels on the cell surface, the mechanisms of which are still poorly understood. Membrane-associating proteins depend on the local spatial distribution of lipids in the plasma membrane (PM) for their function. Here, we report that the highly amphipathic secondary bile acid deoxycholic acid (DCA), a major constituent in the human bile, at doses <1μM enhances the nanoclustering and the PM localization of phosphatidic acid (PA) but disrupts the local segregation of phosphatidylserine in the basolateral PM of the human colorectal adenocarcinoma Caco-2 cells. PA is a key structural component of the signaling nano-domains of epidermal growth factor receptor (EGFR) on the cell surface. We show that DCA promotes the co-localization between PA and EGFR, the PA-driven EGFR dimerization/oligomerization and EGFR signaling. Depletion of PA abolishes the stimulatory effects of DCA on the EGFR oligomerization and signaling. This effect occurs in the cultured Caco-2 cells and the *ex vivo* human intestinal enteroids. We propose a novel mechanism, where the amphiphilic DCA monomers alter the nano-assemblies of anionic phospholipids and in turn change the dynamic structural integrity of the lipid-driven oligomerization of cell surface receptors and their signal transduction.

Introduction

Bile acids are synthesized in the liver, stored in the gallbladder and secreted into the small intestine as a component of the enterohepatic circulation [1]. As biological detergents, the bile acids above their critical micelle concentrations (CMCs) form micelles to emulsify fat-soluble molecules to facilitate digestion of fatty acids and lipids in food. The bile acid micelles also act as vehicles to incorporate endogenous and exogenous hydrophobic waste for excretion. Bile acid concentrations vary widely in human body. Specifically, the secondary bile acid,

and analysis, decision to publish, or preparation of the manuscript.

Competing interests: The authors have declared that no competing interests exist.

deoxycholic acid (DCA), is a major organic component of human bile, comprising 25–35% of all bile content [2]. While the CMC of DCA is 5-7mM in physiological buffer [3], DCA concentration is $< 2\mu M$ in the plasma and in the range of 250–350μM in the colon [2]. At the doses well below their CMCs, the bile acids impact cell signaling cascades, including lipid metabolism, mitogenic signaling, ion channel activation, as well as protein trafficking [4]. These signaling effects contribute to the bile acid-induced pathophysiological conditions, including cholestasis, inflammatory bowel disease and cancer in the GI tract [5, 6]. The ability of bile acids to stimulate the nuclear receptors partially contributes to the bile acid-induced changes in cell function and has been studied extensively [7]. However, how the bile acids activate a variety of cell surface receptors is still poorly understood.

Most membrane-associating surface receptors and ion channels dimerize / oligomerize, which is mediated by the heterogeneous distribution of lipids in the plasma membrane (PM), for their function [8–11]. Although the most well-characterized properties of the bile acids have been their amphiphilicity and their ability to associate with lipids as micelles, the typical physiologically effective doses for the bile acids are well below their CMCs. This implies that interactions between the bile acids and the lipids may not contribute to their biological effects. However, the latest *in vitro* studies using isolated natural PM and synthetic vesicles/planar bilayers show that the bile acid monomers at doses well below their CMCs intercalate in the lipid bilayers and alter the highly dynamic and transient nanometer-scale lateral spatial distribution of the lipids [12–14], without changing the global membrane properties, such as overall membrane permeability and lipid solubility. Thus, it is possible that the bile acids stimulate the cell surface receptors via modulating the structural integrity of the lipid-mediated nano-assemblies of the membrane receptors on the cell surface. Here, we used super-resolution electron microscopy (EM) combined with quantitative spatial analysis to systematically screen how the secondary bile acid, deoxycholic acid (DCA), at doses $<1\mu M$ modulated the nano-segregation of various PM lipids in the basolateral PM of human colorectal adenocarcinoma Caco-2 cells. We then used epidermal growth factor receptor (EGFR) as an example to test the potential consequence of the DCA-induced dimerization/oligomerization and the signaling of EGFR in Caco-2 cells and *ex vivo* human intestinal enteroids.

Results

DCA monomers alter the spatiotemporal organization of plasma membrane phospholipids

Bile acid micelles are effective biological detergents capable of solubilizing lipids and increasing membrane permeability. However, it is not clear how the amphiphilic bile acid monomers at physiological levels potentially influence the much more dynamic nanoscale lipid organization in the PM. As local nanoscale aggregation of the lipids directly participates in the dimerization/oligomerization of the cell surface receptors, the lateral mobility of PM lipids is important for cell signaling [9, 11, 15]. We, thus, tested how DCA influenced the spatial distribution of acidic lipids in the Caco-2 basolateral PM.

We ectopically expressed GFP-tagged lipid binding domains in Caco-2 cells: GFP-LactC2 to label phosphatidylserine (PS) [16], GFP-PASS to label phosphatidic acid (PA) [17], GFP-PH-PLCδ to label phosphoinositol 4,5-bisphosphate (PIP_2) [18], GFP-PH-Akt to label phosphoinositol 3,4,5-trisphosphate (PIP_3) [19] or GFP-D4H to label cholesterol [20]. To eliminate the effect of high levels of bile acids typically present in bovine serum [21], we pre-serum-starved Caco-2 cells for 2h using serum-free EMEM medium before DCA treatment. The spatial organization of each lipid probe was evaluated on intact basolateral PM sheets prepared from the Caco-2 cells using EM-immunogold labeling (S1A and S1B Fig) and univariate

K-function spatial analysis expressed as *L(r)-r* [22, 23]. S1C Fig shows a plot of *L*(*r*)-*r* vs. *r*, where *L*(*r*)-*r* is the extent of nanoclustering and *r* is the length scale in nanometers (nm). *L*(*r*)-*r* values above the 99% confidence interval (99% C.I.) indicate statistically significant clustering, with larger *L*(*r*)-*r* values corresponding to more extensive clustering. The peak *L*(*r*)-*r* value, L_{max}, of each curve summarizes the clustering data (Fig 1A).

We found that DCA markedly enhanced PA nanoclustering and disrupted PS clustering, while having little effect on PIP_2, PIP_3 and cholesterol (Fig 1A). By counting the number of the gold nanoparticles per $1\mu m^2$ PM area, we estimated changes in level of each type of lipids in the PM. DCA markedly elevated the level of PA but decreased the level of PIP_2 in the PM of Caco-2 cells (Fig 1B). Changes in the PM lipid levels were unlikely to be caused by alterations in lipid metabolism because of the short DCA treatment time; DCA incubation of at least 1h is required to induce any meaningful change in lipid metabolism [24]. Further, DCA caused no change in cholesterol aggregation pattern and PM level (Fig 1A and 1B), consistent with the view that changes lipid levels observed in Fig 1 were independent of lipid metabolism.

Conjugated bile acids are typically more hydrophilic than their unconjugated cognates, thus possessing less ability to influence PM lipids [1]. We then tested how taurine-conjugated DCA, taurodeoxycholic acid (TDCA), potentially influenced the spatial segregation of PA. We focused specifically on PA because DCA-induced elevation in PA clustering was the most striking. S1D Fig shows that TDCA had minimal effect on the clustering of PA. Interestingly, TDCA treatment induced significant mis-localization of PA from the PM of Caco-2 cells (S1E Fig). Ursodeoxycholic acid (UDCA) and its conjugated cognate tauroursodeoxycholic acid (TUDCA) have been shown to be cytoprotective [1]. S1D and S1E Fig show that either UDCA or TUDCA had no effect on PA clustering, but mis-localized PA from the PM. To further examine the well-documented cytoprotective effects of UDCA against DCA, we conducted similar EM-spatial analysis using Caco-2 cells treated with DCA alone, UDCA alone or combination of both DCA and UDCA. S1F and S1G Fig show that co-treatment with 1μM DCA and 1μM UDCA completely abolished the enhancing effects of DCA alone on PA clustering and PM localization.

To further explore the dynamics of the DCA effect on PA, we conducted EM-spatial analysis in a time course experiment. DCA at 1μM enhanced PA nanoclustering and PM localization within 30 seconds, achieved a peak effect within 5 minutes, and returned to the baseline within 20 minutes (Fig 1C and 1D). We next conducted dose response experiments by incubating Caco-2 cells with different concentrations of DCA (0.05–30μM) for 5 minutes. PA nanoclustering and PM level were elevated at 0.05μM and plateaued at ~1μM DCA (EC_{50} ~ 0.6μM, Fig 1E and 1F).

Bile acid enhances EGFR dimerization/oligomerization

PA is a major structural component of EGFR signaling nanoclusters and mediates EGFR--MAPK signal transmission [15, 17, 25]. DCA robustly activates EGFR-dependent MAPK signaling in many GI cell lines [24, 26, 27]. We then used EGFR as an example to examine how the DCA-induced changes in PM lipids potentially contribute to the function of the surface receptors. EM-spatial analysis revealed that DCA at 1μM enhanced EGFR-GFP nanoclustering and PM localization within 30 seconds, an effect that peaked at ~5 minutes (Fig 1C and 1D). DCA at low doses (EC_{50} ~ 0.3μM and plateau at ~1μM) robustly elevated EGFR nanoclustering and PM localization (Fig 1E and 1F). Because EGFR dimerization/oligomerization is an essential step in EGFR signaling [9, 10], we further interrogated our spatial data and evaluated the potential effects of DCA on population distribution of EGFR in the PM. DCA at 1μM for 5 minutes decreased the EGFR monomer population, while significantly elevating the dimer

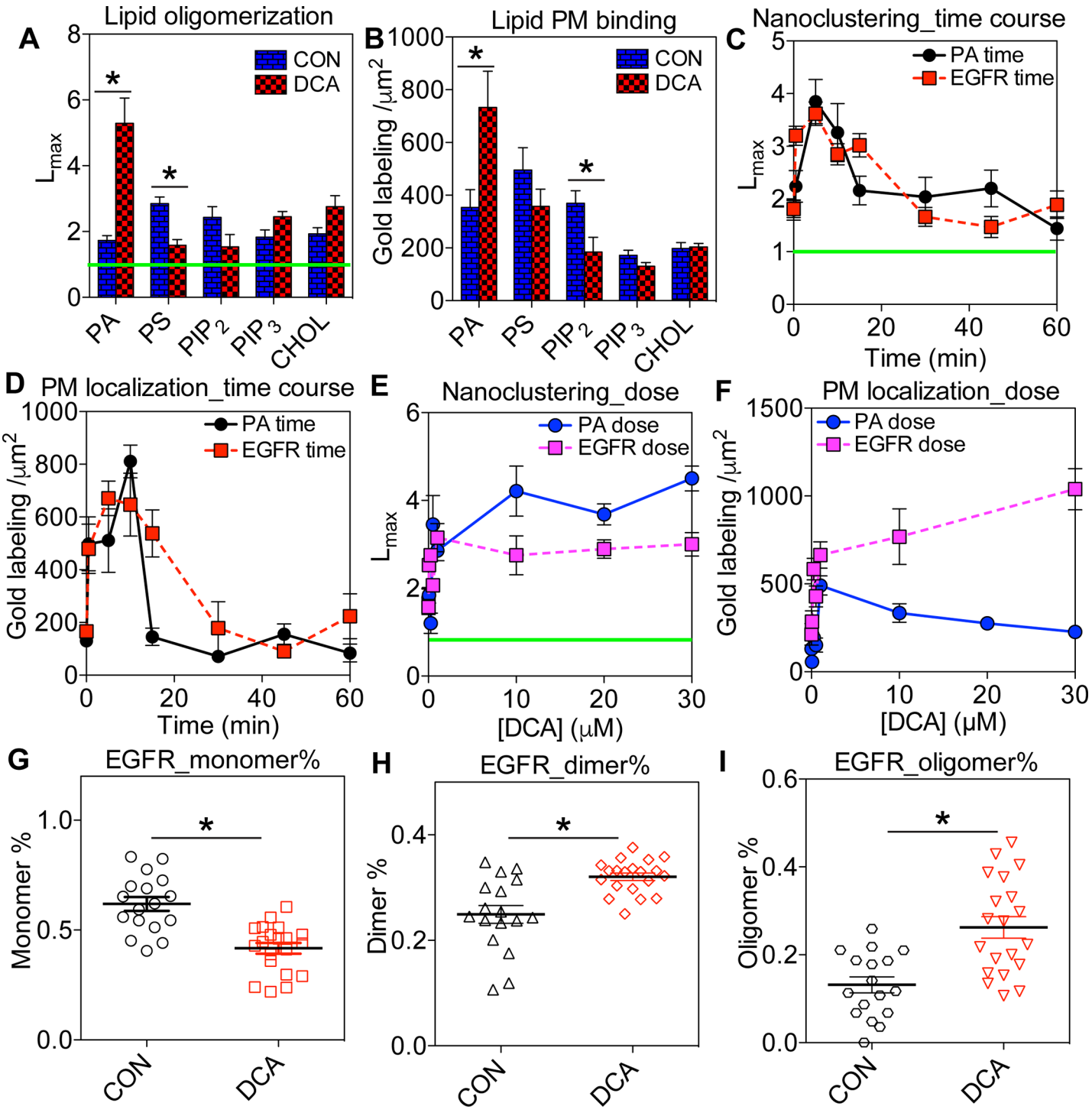

Fig 1. DCA alters the dynamic spatial distribution of various lipids and EGFR in Caco-2 basal PM. (A) Caco-2 cells ectopically expressing a GFP-tagged lipid-binding domain were treated with 1μM DCA for 5 minutes. Intact basolateral PM sheets of Caco-2 cells were then attached to EM grids and immunolabeled with 4.5nm gold nanoparticles conjugated to anti-GFP antibody. Gold particles were imaged via transmission EM (TEM) at 100,000X magnification. Spatial distribution of gold particles within a 1μm^2 PM area was quantified using univariate K-function. L_{max} values above 1 indicate statistically meaningful clustering, whereas L_{max} values below 1 indicate spatial uniformity. (B) Number of gold particles within the same 1μm^2 PM area was counted as an estimate of lipid level in the PM. (C and D) Caco-2 cells expressing either GFP-PASS (to specifically tag PA) or EGFR-GFP were exposed to 1μM DCA for various time points (0–60 minutes) before immunogold labeling. Extent of univariate spatial distribution (C) and number of gold labeling (D) of GFP-PASS or EGFR-GFP were calculated as described above. (E and F) Caco-2 cells ectopically expressing GFP-PASS or EGFR-GFP were exposed to increasing concentrations of DCA (0–30μM) for 5 minutes before immunogold labeling. Spatial distribution (E) and number of gold particles within a 1μm^2 PM area (F) were calculated. Changes in EGFR monomer (G), dimer (H) and oligomer (I) populations

without / with 1μM DCA were calculated using the spatial analysis data. At least 15 PM sheets from individual cells were analyzed in each condition. Statistical significance of the univariate clustering analysis (*A*, *C* and *E*) was evaluated via comparing our data against 1000 bootstrap tests, with * indicating $p<0.05$. One-way ANOVA was performed to evaluate statistical significance in gold labeling number data (*B*, *D* and *F*), with * indicating $p<0.05$. Statistical significance of EGFR population distribution between untreated and DCA-treated conditions (*G-I*) was evaluated using one-way ANOVA with * indicating $p<0.05$.

https://doi.org/10.1371/journal.pone.0198983.g001

and the oligomer populations of EGFR (Fig 1G–1I). Thus, effects of DCA on EGFR nanoclustering correlated well with its effects on PA clustering in both the time course and dose response studies.

DCA enhances co-localization between EGFR and PA in Caco-2 basal PM

To further establish causality, we quantified the co-localization between the acidic lipids and EGFR in the Caco-2 basal PM using the bivariate EM co-localization analysis. The basal PM of Caco-2 cells co-expressing one of the GFP-tagged lipid binding domains and EGFR-RFP were attached to the EM grids and co-immunolabeled with both 6nm gold nanoparticles linked to anti-GFP antibody and 2nm gold nanoparticles coupled to anti-RFP antibody. The spatial distribution of the two populations of gold particles was imaged using TEM and analyzed using the bivariate K-functions (S2A and S2B Fig). S2C Fig shows the extent of co-localization, $L_{biv}(r)$-r, plotted against the length scale, r. The $L_{biv}(r)$-r values above the 95%C.I. of 1 indicate the statistically significant co-localization between the 6nm and 2nm gold populations. To summarize the co-localization data, we calculated the area-under-the-curve for the $L_{biv}(r)$-r curves and termed as the L-bivariate integrated, or LBI. The high LBI values indicate more extensive co-localization while the LBI values <100 indicate no co-localization between the two gold populations [22, 23]. Fig 2A shows the LBI values for the extent of co-localization between EGFR and various lipids. Interestingly, in the untreated Caco-2 cells, EGFR co-localized extensively with cholesterol (Fig 2A); DCA at 1μM for 5 minutes markedly elevated the co-localization between EGFR and PA, while depleting cholesterol from the EGFR nanoclusters (Fig 2A). Although DCA further decreased the LBI value between EGFR and PIP_3, this decrease was not biological meaningful because both LBI values between EGFR and PIP_3 in the absence or presence of DCA were below the confidence interval (Fig 2A). DCA had little effect on the association of EGFR with PS or PIP_2. Taken together, our data suggest that DCA has distinct local effects on the lipid composition of EGFR nanoclusters in the PM.

EGFR interacts with lipids in the PM via a single-span transmembrane domain (TMD) and an adjacent intracellular juxtamembrane domain (JMD) enriched with basic residues [9, 28]. To further examine whether the DCA-enhanced EGFR oligomerization is a membrane-mediated effect, we ectopically expressed a GFP-tagged truncated EGFR containing only the TMD and the JMD (amino acids 622–663), termed as TMD_JMD-GFP, in the Caco-2 cells. In the absence of all the extracellular domains and the intracellular phosphorylation sites, TMD_JMD-GFP is likely only sensitive to changes in the nano-environment of the PM. We then compared the ability of DCA to alter the oligomerization pattern of the full-length EGFR-GFP vs. the truncated TMD_JMD-GFP by performing the immunogold EM-univariate spatial analysis. Fig 2B shows that, in the basal PM of the untreated Caco-2 cells, TMD_JMD-GFP clustered as efficiently as the full-length EGFR-GFP. The clustering of TMD_JMD-GFP also responded to DCA (1μM, 5 minutes) as effectively as its full-length cognate (Fig 2B). Upon dimerization, the helical structure of the EGFR JMD of each monomer associates extensively with the anionic lipids in the PM using exposed basic residues, such as Arginine (Arg) 651, Arg657 and Arg662 [11]. The basic residues Arg645-647 also participate in binding with the anionic lipids in the membranes [8]. We, therefore, mutated Arg647, Arg651 and Arg662 to the neutral alanines to generate a triple alanine mutant TMD_JMD_3A-GFP. In an EM-

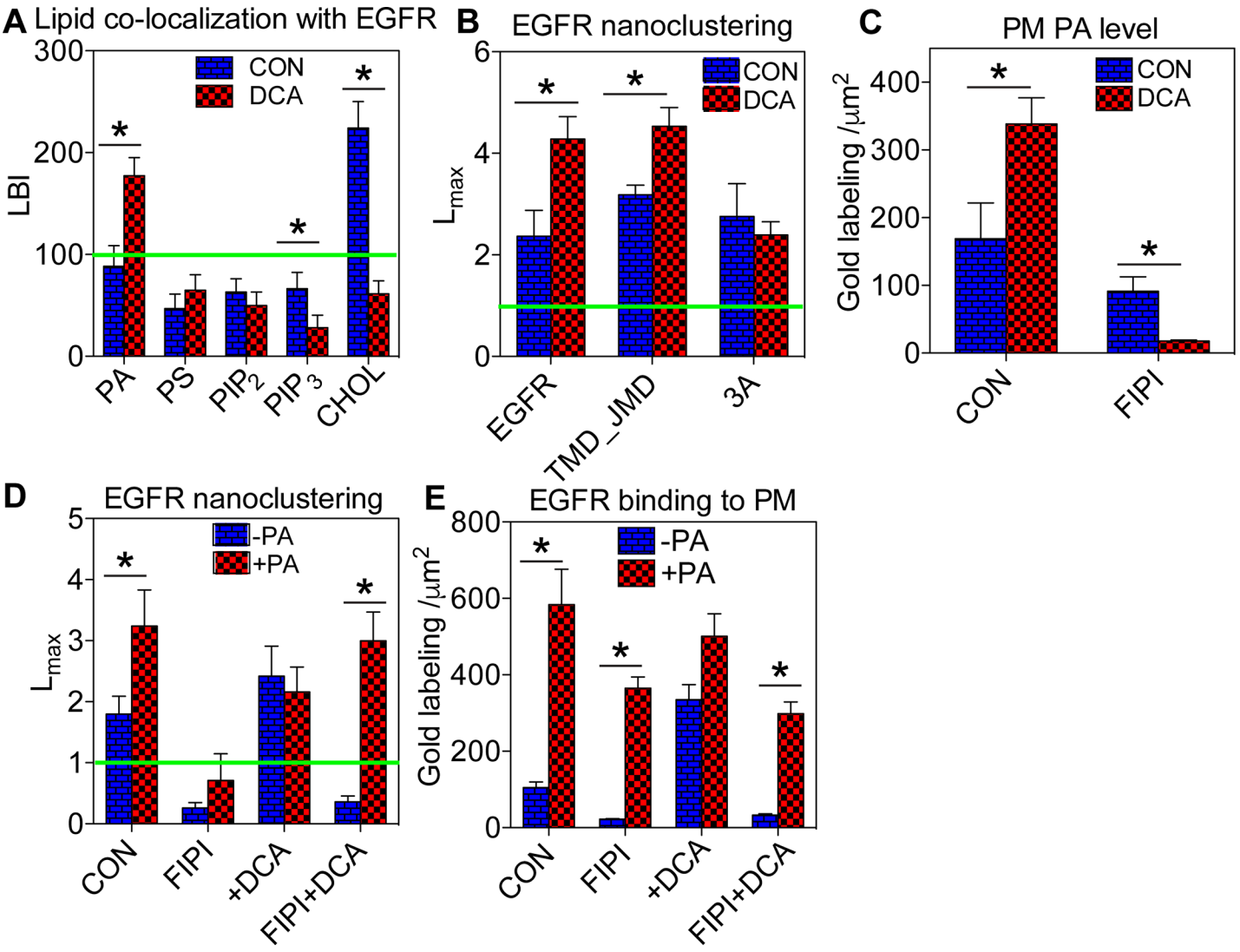

Fig 2. DCA-induced elevation of EGFR oligomerization in Caco-2 PM is mediated by PA. (A) Co-localization between various lipid-binding domains and EGFR was quantified using EM-bivariate co-localization analysis. Caco-2 cells co-expressing a GFP-tagged lipid-binding domain and EGFR-RFP were grown to a monolayer before treatment of 1μM DCA for 5 minutes. Intact basal PM of Caco-2 cells was attached to EM grids and immunolabeled with 6nm gold nanoparticles conjugated with anti-GFP antibody and 2nm gold linked to anti-RFP antibody, respectively. Gold distribution was imaged using TEM at 100,000x magnification and analyzed using bivariate K-function. LBI values indicate extent of co-localization between each lipid type and EGFR, with values >100 indicating statistically significant co-localization. (B) EM-univariate spatial analysis shows the extent of oligomerization of the full-length EGFR-GFP, the truncated transmembrane domain/juxtamembrane domain TMD_JMD-GFP, and the truncated mutant TMD_JMD_3A-GFP in the basal PM of Caco-2 cells without / with 1μM DCA for 5 minutes. (C) Caco-2 cells expressing GFP-PASS (specifically binding to PA) were pre-treated with 0.75μM FIPI (pan-PLD inhibitor) for 25 minutes before co-incubation with both 0.75μM FIPI and 1μM DCA for an additional 5 minutes. In the same EM-spatial analysis, the number of gold particles with a 1μm^2 PM area was counted to estimate changes in PA level in the cell PM. The same PA depletion experiments using FIPI were conducted on Caco-2 cells expressing EGFR-GFP without / with supplementation of 10μM exogenous egg PA. Oligomerization (D) and number of gold particles (E) within a 1μm^2 PM area were quantified using EM-univariate clustering analysis. For all the EM-immunogold labeling univariate and bivariate experiments, at least 15 PM sheets from individual cells were analyzed in each condition. In all univariate and bivariate spatial analyses (*A*, *B*, *C*, and *E*), statistical significance between untreated controls and various treatments in clustering analyses was evaluated using bootstrap tests, with * indicating $p<0.05$. Statistical significance of gold numbers (*D* and *F*) was evaluated using one-way ANOVA, with * indicating $p<0.05$.

https://doi.org/10.1371/journal.pone.0198983.g002

univariate analysis, TMD_JMD_3A-GFP no longer responded to the DCA stimulation (Fig 2B). Thus, our data suggests that EGFR JMD association with the anionic lipids in the PM mediates DCA-induced EGFR oligomerization.

To further investigate the role of PA in the DCA-enhanced EGFR nanoclustering, we pre-treated the Caco-2 cells with 5-fluoro-2-indolyl des-chlorohalopemide (FIPI), a

pharmacological inhibitor of phospholipase D (PLD) that catalyzes the conversion of phosphatidylcholine (PC) to PA [17], before co-incubation with 1μM DCA. The FIPI treatment effectively abolished the ability of DCA to elevate PA levels in the Caco-2 PM (Fig 2C). The FIPI treatment also disrupted EGFR oligomerization and PM localization and effectively abolished the DCA-induced elevation of EGFR oligomerization/PM localization (Fig 2D and 2E). Supplementation with the exogenous egg PA effectively reversed the FIPI inhibitory effects (Fig 2D and 2E). Our data suggest that the lipid messenger PA mediates the DCA-induced changes in EGFR oligomerization in the Caco-2 PM.

PA mediates DCA-stimulation of EGFR-MAPK signaling

We then quantified the signaling effects of DCA on EGFR signaling. In a time-course study, the Caco-2 cells were serum-starved and then incubated with 1μM DCA for various time periods before harvesting. Western blotting was then used to quantify the ability of DCA to stimulate the phosphorylation of MEK/ERK in the MAPK pathway, as well as the phosphorylation of Akt in the PI3K pathway. Fig 3A shows that DCA robustly elevated the levels of pMEK and pERK in the Caco-2 cells within 2–5 minutes, which decayed to the baseline within 15 minutes. This robust activation is consistent with the previous findings [24, 26, 27], and is also consistent with the time-course of DCA-elevated oligomerization of the EGFR (Fig 1C and 1D). In a dose response study, the MAPK signal output was elevated by 50nM DCA and plateaued at ~1μM with an EC50 of ~0.2μM (Fig 3B). The effective DCA doses for stimulating the EGFR-MAPK signaling were significantly lower than previously shown, but consistent with the effective DCA doses required to elevate the oligomerization of EGFR (Fig 1E and 1F). DCA did not change the pAkt level in either the time course or the dose experiments, suggesting that DCA has no measurable effect on the PI3K pathway in Caco-2 cells.

The essential role of EGFR in the DCA-induced stimulation of the MAPK signaling has been shown before [24, 26, 27]. We also validated this via pre-treating the Caco-2 cells with a specific EGFR inhibitor AG1478 before the DCA exposure. The AG1478 pre-treatment completely abolished the stimulatory effects of DCA (S2D Fig), showing that DCA specifically targets EGFR. Concordantly DCA had no effect on the MAPK signaling in the wild-type Chinese hamster ovarian (CHO) cells, which do not possess the endogenous EGFR [29], but effectively elevated the MAPK signaling in the CHO cells stably expressing EGFR-GFP (S2E Fig). These data clearly show the essential role of EGFR in the DCA-stimulation of the mitogenic signaling. Depletion of the endogenous PA via the FIPI treatment significantly abrogated the ability of DCA to stimulate the EGFR/MAPK signaling (Fig 3C). Taken together, these data suggest that generation of PA mediates the DCA stimulation of the EGFR-MAPK pathway.

PA mediates DCA stimulation of EGFR signaling in ex vivo human intestinal enteroids

To further examine the physiological relevance of PA in mediating the effects of DCA, we conducted signaling experiments using *ex vivo* human intestinal enteroids. De-identified intestinal biopsies were obtained and enteroid cultures were established from isolated intestinal crypts [30–32]. Under controlled conditions, established ex vivo enteroid cultures maintained in Matri gel were differentiated to express the intestinal epithelial cell types that recapitulate functions of an intact intestine [30–32]. We first conducted the time-course and the dose response experiments using the human intestinal enteroids; similar to Caco-2 cells, DCA rapidly elevated the MAPK signaling which peaked at 5 minutes and returned back to the baseline within 15 minutes (Fig 4A). The DCA dose response plateaued at ~5μM (Fig 4B). Pre-treatment with the pan-PLD inhibitor FIPI effectively abolished the ability of DCA to activate the MAPK

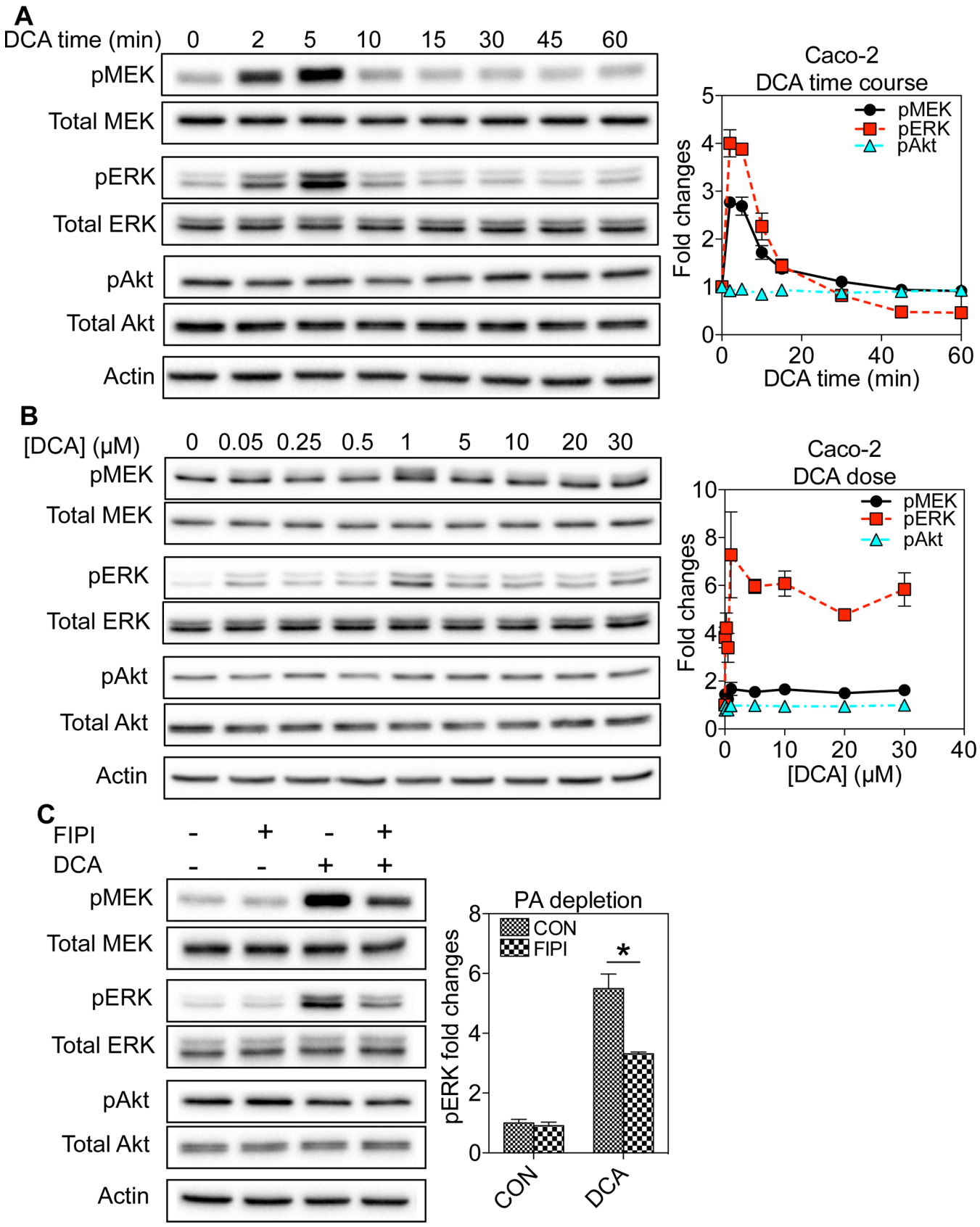
A
DCA time (min) 0 2 5 10 15 30 45 60
pMEK
Total MEK
pERK
Total ERK
pAkt
Total Akt
Actin
Caco-2
DCA time course
pMEK
pERK
pAkt
Fold changes
DCA time (min)
B
[DCA] (μM) 0 0.05 0.25 0.5 1 5 10 20 30
pMEK
Total MEK
pERK
Total ERK
pAkt
Total Akt
Actin
Caco-2
DCA dose
pMEK
pERK
pAkt
Fold changes
[DCA] (μM)
C
FIPI - + - +
DCA - - + +
pMEK
Total MEK
pERK
Total ERK
pAkt
Total Akt
Actin
PA depletion
CON
FIPI
*
pERK fold changes
CON
DCA

Fig 3. DCA stimulation of EGFR-MAPK signaling in Caco-2 cells is mediated by PA. (A) Caco-2 cells grown to a monolayer were pre-serum-starved before incubation with 1μM DCA for various time points to ensure that the total serum starvation time was 3 hours without / with DCA. Whole cell lysates were collected and blotted using antibodies against pMEK, total MEK, pERK, total ERK, pAkt or total Akt, as well as the loading control actin. (B) Caco-2 cells grown to a monolayer were pre-serum-starved for 2 hours and 55 minutes before incubation with various concentrations (1–30μM) DCA for 5 minutes. Whole cell lysates were collected and blotted using antibodies against pMEK, total MEK, pERK, total ERK, pAkt or total Akt, as well as the loading control actin. (C) Caco-2 cells were pre-serum-starved for 2 hours and 30 minutes before incubation with 0.75μM FIPI for 25 minutes and subsequent co-incubation with FIPI and 1μM DCA for 5 minutes. Whole cell lysates were collected for Western blotting against pMEK, total MEK, pERK, total ERK, pAkt or total Akt, as well as the loading control actin. In all signaling experiments, 3 individual experiments were performed separately and quantitation is shown as mean±SEM. Statistical significance was evaluated using one-way ANOVA, with * indicating $p<0.05$.

https://doi.org/10.1371/journal.pone.0198983.g003

signaling (Fig 4C). Taken together, DCA had a similar ability to enhance the PA-mediated EGFR-MAPK signaling in the *ex vivo* human tissue.

DCA modulates lipid dynamics and cell signaling in non-GI cells in a similar manner

Low levels of the bile acids (<5μM), of which ~30% can be DCA, can be found in the circulation [2]. Our data showing that DCA at doses <1μM robustly enhanced EGFR oligomerization and signaling in the GI cells and tissues suggest that a similar behavior can occur in non-GI cells/tissues. To test this, we first conducted the time-course and the dose studies to examine how DCA potentially influence the EGFR-MAPK and the PI3K cascades in the baby hamster kidney (BHK) cells (S3A and S3B Fig). The time-course for the DCA stimulation of the MAPK pathway in the BHK cells was similar to the Caco-2 cells (S3A Fig). Strikingly, DCA effectively decreased the pAkt levels by >50% within 5 minutes (S3A Fig), suggesting effective inhibition of the PI3K pathway by DCA in the BHK cells. We also validated the EGFR-dependence by pre-treating the BHK cells with AG1478. As expected, inhibiting the EGFR activity effectively abolished the DCA stimulation of the EGFR-MAPK signaling (S3C Fig). To examine if DCA affected the EGFR oligomerization in the BHK cells, we conducted the EM-univariate clustering analysis. The spatial analysis showed that DCA enhanced the oligomerization of EGFR-GFP in the apical PM of the BHK cells (S3D Fig). Taken together, our data suggest that DCA has the similar stimulatory effects on the EGFR/MAPK signaling in non-GI cells. The PI3K pathway, on the other hand, responded differently in the Caco-2 cells vs. the BHK cells, suggesting the potential tissue-specific responses.

Discussion

Our current study aims to explore potential molecular mechanism(s) for the bile acid-induced activation of the cell surface EGF receptor. We found that the secondary bile acid DCA has selective effects on the spatial distribution of different acidic lipids in the PM of the Caco-2 cells. Especially, DCA markedly enhances the local spatial aggregation of PA, which in turn induces the co-localization between PA and EGFR, promotes the EGFR dimerization/oligomerization and stimulates the EGFR-MAPK signaling. Acute PA depletion effectively abolishes the DCA-induced EGFR oligomerization and the DCA stimulation of the EGFR-MAPK signaling. This effect has been observed in both the cultured human colon cancer cell line and the *ex vivo* human intestinal enteroids. Thus, the dynamic nano-domains of the anionic lipids in the PM may act as the signaling platforms to mediate the bile acid stimulation of the cell surface receptors.

Dependence of the EGFR oligomerization on the acidic lipids has been demonstrated before. The EGFR likely engages with PM lipids via the hydrophobic single-span TMD and the adjacent intracellular JMD enriched with positively charged residues [8, 15, 33]. Indeed, a truncated EGFR fragment containing only the TMD and JMD clusters as efficiently as the full-

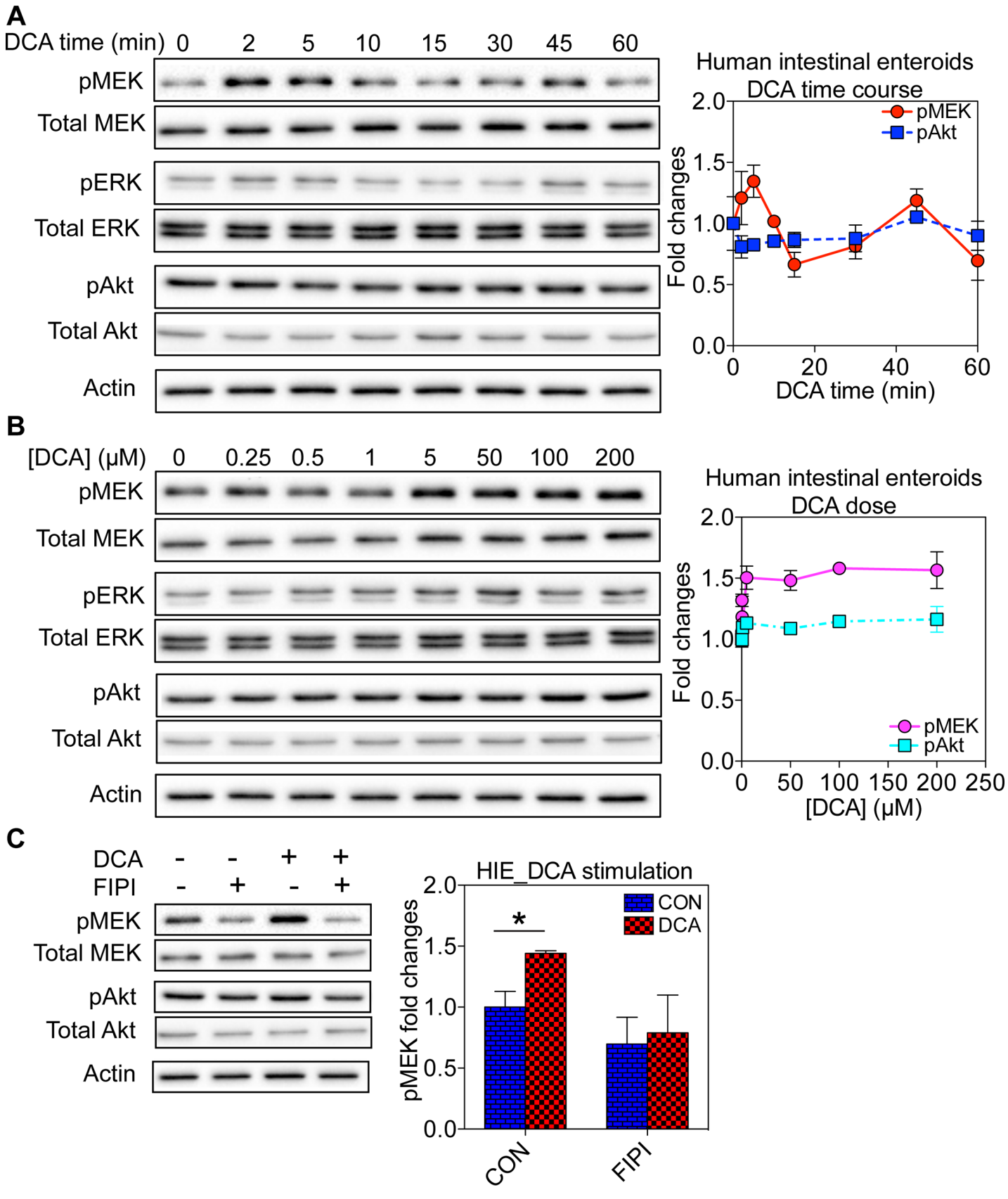
A
DCA time (min) 0 2 5 10 15 30 45 60
pMEK
Total MEK
pERK
Total ERK
pAkt
Total Akt
Actin
Human intestinal enteroids
DCA time course
pMEK
pAkt
Fold changes
DCA time (min)
B
[DCA] (μM) 0 0.25 0.5 1 5 50 100 200
pMEK
Total MEK
pERK
Total ERK
pAkt
Total Akt
Actin
Human intestinal enteroids
DCA dose
Fold changes
pMEK
pAkt
[DCA] (μM)
C
DCA - - + +
FIPI - + - +
pMEK
Total MEK
pAkt
Total Akt
Actin
HIE_DCA stimulation
CON
DCA
pMEK fold changes
*
CON
FIPI

Fig 4. DCA stimulation of EGFR-MAPK signaling in *ex vivo* human intestinal enteroids is mediated by PA. (A) Human intestinal enteroids were pre-serum-starved before incubation with 5 μM DCA for various time points to ensure total serum starvation time is 2 hours for all conditions. Whole cell lysates were collected and blotted using antibodies against pMEK, total MEK, pERK, total ERK, pAkt or total Akt, as well as the loading control actin. (B) Human intestinal enteroids were serum-starved for 1 hour and 55 minutes before incubation with 1–200μM DCA for an additional 5 minutes. Whole cell lysates were collected and blotted using antibodies against pMEK, total MEK, pERK, total ERK, pAkt or total Akt, as well as the loading control actin. (C) Pre-serum-starved human intestinal enteroids were treated with 0.75μM FIPI for 25 minutes and subsequent co-incubation with both FIPI and 5μM DCA. Whole cell lysates were collected and blotted using antibodies against pMEK, total MEK, pERK, total ERK, pAkt or total Akt, as well as the loading control actin. In all signaling experiments, 3 individual experiments were performed separately and quantitation is shown as mean±SEM. Statistical significance was evaluated using one-way ANOVA, with * indicating $p<0.05$.

https://doi.org/10.1371/journal.pone.0198983.g004

length EGFR in the PM (Fig 2C). Binding to the acidic lipids via the polybasic sequences in its JMD drives allosteric folding of the EGFR cytoplasmic domain, which is a key step in the EGFR dimerization/oligomerization and the consequential auto-phosphorylation and the activation [8, 15, 33]. Specifically, EGFR preferentially associates with PA and depends on PA interactions for the oligomerization and the signal transduction [15]. Concordantly, mutating the basic residues in the JMD significantly compromises the ability of DCA to elevate EGFR oligomerization (Fig 2B). Thus, altering the local spatial distribution of PM lipids surrounding EGFR potentially changes EGFR activities. By contrast, PS, also a monovalent anionic phospholipid, has no effect on the EGFR oligomerization [15], suggesting that EGFR possesses specific lipid sorting capacity rather than simply sensing global electronegativity on the PM.

It is also interesting that DCA induces local cholesterol depletion from EGFR, while EGFR co-localizes with cholesterol extensively in the untreated Caco-2 cells. The role of cholesterol in regulating the EGFR activation is controversial. While some studies show that cholesterol inhibits the EGFR ligand-independent activation [28], others propose that cholesterol positively regulates the EGFR stimulation [34]. Our current data suggest that cholesterol content surrounding EGFR is highly transient. While EGFR co-localizes with cholesterol extensively at the basal state, cholesterol is depleted from EGFR upon the DCA incubation. Although our data is consistent with the inhibitory effects of cholesterol on EGFR, we cannot rule out the possibility that cholesterol enrichment at the basal state is still required for its proper activation.

It is not entirely clear how DCA specifically targets PA in the PM. Amphipathic bile acids, such as DCA, possess the capability to intercalate in the PM and shift the lateral distribution of the lipids. Indeed, recent biophysical studies show that DCA at low concentrations well below its CMC preferentially partitions into highly fluid liquid-disordered domains and induces further phase separation in synthetic and isolated native membranes [12, 13]. DCA at <15μM also induces marked changes in the cross-sectional area of lipids in monolayers [14]. These *in vitro* studies show that DCA monomers drive the immiscibility of lipids with distinct acyl chain lengths and unsaturation levels, which induces the formation of co-existing domains in the membranes. Because mammalian cells contain many PA species with various acyl chain structures [35] and DCA preferentially partitions into highly fluid domains containing lipids with polyunsaturated tails [12, 13], DCA intercalation may preferentially drive the spatial segregation among different PA species with distinct tail structures. This may contribute to the elevation in PA clustering observed in the current study. Thus, the lateral distribution of PA lipids may be altered as a result of DCA-enhanced heterogeneity of the PM. Furthermore, because of the changes in the PA levels in the PM upon DCA treatments in our EM immunogold labeling analysis, it is also possible that DCA may directly target PLD activities to stimulate the local generation of PA in the PM. It is likely that both biophysical DCA / PM lipid association and DCA / PLD interactions mediate the bile acid-induced elevation in PA generation in the PM. Further studies are required to deduce detailed mechanisms for bile acid-induced changes in the dynamics of PM lipids.

In addition to PA, DCA also significantly disrupts PS clustering and mislocalizes PIP_2 from the basal PM of the Caco-2 cells. Although not clear of the underlying mechanisms, these effects may influence cell functions dependent on these lipids. Since DCA does not alter the co-localization between EGFR and PS or PIP_2 (Fig 2A), it is unlikely that these two lipids participate in the DCA-enhanced oligomerization of EGFR. However, both PS and PIP_2 contribute to the function of several downstream constituents of EGFR. For instance, PIP_2 is a substrate of PI3K, which converts PIP_2 to PIP_3. Thus, DCA-induced mislocalization of PIP_2 in the PM may attenuate PI3K signaling. This mechanism may contribute to the DCA-induced inhibition of Akt phosphorylation in BHK cells observed in the current study (S3 Fig). PIP_2 also regulates or inhibits functions of many ion channels on the cell PM. Particularly, many cholestatic patients with elevated serum bile acid levels suffer debilitating itch [36], mechanism of which is still unknown. Transient receptor potential Ankyrin sub-family 1 (TRPA1) is the ion channel mostly implicated in chronic itching [36]. PIP_2 associates with TRPA1 and inhibits its channel function [37]. Thus, DCA can potentially activate TRPA1 channels and cause chronic itching partially via depleting local PIP_2 level, although bile acid specific receptor TGR5 has also been implicated [38].

Conclusion

Here we propose that the secondary bile acid, DCA, stimulates EGFR-MAPK signaling via modulating the dynamic spatial distribution of minor acidic lipids in the PM. DCA has distinct effects on different PM lipids, which potentially leads to highly diverse responses from various lipid-dependent surface receptors, ion channels and other membrane-associating proteins. This lipid-mediated effect potentially contributes to the diverse biological and pathophysiological effects of bile acids.

Experimental procedures

Electron microscopy (EM)-spatial analysis

EM-univariate clustering analysis. The univariate spatial analysis quantifies the extent of nanoclustering of a single species of immunogold-labeled constituent on cell PM. Caco-2 cells ectopically expressing GFP-tagged lipid-binding domains or EGFR were seeded on gold EM grids and grown to a monolayer. After treatment of DCA at various doses and time points under physiological condition (37˚C and 5% CO_2), the apical portion of the cells was peeled off using a filter paper wetted with PBS, leaving only intact basolateral PM attached to the gold EM grids. Basal PM was then fixed in 4% paraformaldehyde (PFA) and 0.1% gluaraldehyde, immunolabeled with 4.5nm gold nanoparticles conjugated to anti-GFP antibody and negative-stained with uranyl acetate at room temperature. Gold particles on intact basal PM was imaged using TEM at 100,000x magnification. The coordinates of each gold particle were assigned using ImageJ. Spatial distribution of gold particles was quantified using Ripley's K-function, which tests the null hypothesis that all points in a selected area are distributed randomly (Eqs 1 and 2):

$$K(r) = An^{-2} \sum_{i \neq j} w_{ij} 1(\|x_i - x_j\| \leq r) \quad (1)$$

$$L(r) - r = \sqrt{\frac{K(r)}{\pi}} - r \quad (2)$$

where $K(r)$ = univariate K-function for a distribution of n gold particles in a basal PM area of A; r = length scale between 1 and 240 nm at 1nm increments; $\|\cdot\|$ = Euclidean distance;

indicator function of 1(·) is assigned a value of 1 if $||x_i\text{-}x_j|| \leq$ r and is assigned a value of 0 if $||x_i\text{-}x_j|| >$ r. An unbiased edge correction for points at the edge of the study area was achieved via including w_{ij}^{-1} = the proportion of the circumference of a circle that has the center at x_i and radius $||x_i\text{-}x_j||$. $L(r)$—r is a linear transformation of $K(r)$ and is normalized against the 99% confidence interval (99% C.I.) estimated from Monte Carlo simulations. Points distributed in a complete random manner yields a $L(r)$—r value of 0 for all values of r. On the other hand, spatial clustering at certain length scale yields a $L(r)$—r value above the 99% C.I. of 1 at the corresponding value of r. At least 15 PM sheets were imaged, analyzed and pooled for each condition in the current study. Statistical significance was evaluated via comparing our calculated point patterns against 1000 bootstrap samples in bootstrap tests [39].

Population distribution was calculated via counting the numbers of gold nanoparticles within a distance of 15nm. A single gold particle found within 15nm distance was categorized as a monomer, while more than 3 gold particles found within 15nm were categorized as oligomers.

EM-Bivariate co-localization analysis. The bivariate co-localization analysis quantifies co-clustering / co-localization between GFP-tagged and RFP-tagged of proteins / peptides on the PM inner leaflet. This bivariate analysis allows quantification of co-localization over a wide range of distances between 8-240nm. Intact basal PM of Caco-2 cells co-expressing both populations of proteins was attached and fixed to EM grids. GFP- and RFP-tagged proteins on the intact basal PM sheets were immunolabeled with 2nm gold conjugated to anti-RFP antibody and 6nm gold linked to anti-GFP antibody. X and Y coordinates to each population of gold particles were assigned using ImageJ. Gold particle co-localization was calculated using a bivariate K-function, which tests the null hypothesis that the two point populations spatially segregate from each other. (Eqs 3–6):

$$K_{biv}(r) = (n_b + n_s)^{-1}[n_b K_{sb}(r) + n_s K_{bs}(r)] \tag{3}$$

$$K_{bs}(r) = \frac{A}{n_b n_s}\sum_{i=1}^{n_b}\sum_{j=1}^{n_s} w_{ij} 1(\|x_i - x_j\| \leq r) \tag{4}$$

$$K_{sb}(r) = \frac{A}{n_b n_s}\sum_{i=1}^{n_s}\sum_{j=1}^{n_b} w_{ij} 1(\|x_i - x_j\| \leq r) \tag{5}$$

$$L_{biv}(r) - r = \sqrt{\frac{K_{biv}(r)}{\pi}} - r \tag{6}$$

where $K_{biv}(r)$ = the bivariate estimator composed of 2 individual bivariate K-functions: $K_{bs}(r)$ for the distribution of the 6nm-big gold particles (b = big gold) with respect to each 2nm-small gold particle (s = small gold); and $K_{sb}(r)$ for the distribution of the small gold particles with respect to each big gold particle. An intact PM sheet with an area A contains n_b, number of 6nm big gold particles and n_s, number of 2nm small gold particles. Other notations are the same as in Eqs 1 and 2 above. $L_{biv}(r)$-r is a linear transformation of $K_{biv}(r)$, and was normalized against the 95% confidence interval (95% C.I.) estimated from Monte Carlo simulations. Spatial segregation between the two populations of gold particles yields an $L_{biv}(r)$-r value of 0 for all values of r. On the other hand, co-localization that occurs at certain distance yields an $L_{biv}(r)$-r value above the 95% C.I. of 1 at the corresponding distance of r. Each $L_{biv}(r)$-r curve was then integrated to yield a value of area-under-the-curve over a fixed range $10 < r < 110$

nm, which was termed bivariate $L_{biv}(r)$-r integrated (or LBI):

$$LBI = \int_{10}^{110} Std\ L_{biv}(r) - r.dr \quad (7)$$

For each condition, at least 15 basal PM sheets were imaged, analyzed and pooled to show as mean of LBI values ± SEM. Statistical significance between conditions was evaluated via comparing against 1000 bootstrap samples as described [39].

Cultured cells and Western blotting

Caco-2 cells were grown in EMEM containing 20% FBS until a monolayer formed. BHK cells were grown in DMEM containing 10% BCS until 85–90% confluency. CHO cells were grown DMEM containing 10% FBS until 85–90% confluency. All cultured cells were pre-serum-starved before DCA treatment in all experiments. In all time course, dose dependence and inhibition studies, total serum starvation time was kept the same for all conditions for each cell line. Specifically, total serum starvation time was 3 hours for Caco-2 cells, 2 hours for BHK cells and 2 hours for CHO cells.

Whole cell lysates were collected and blotted using antibodies against pMEK, pERK and pAkt. Actin was used as loading control. Each experiment was performed at least 3 times separately and data was shown as mean±SEM. Statistical significance was evaluated using one-way ANOVA, with * indicating $p < 0.05$.

Human intestinal enteroids

Handling of human intestinal enteroids was the same as described before [31]. Briefly, de-identified human intestinal biopsies were obtained and used to isolate intestinal crypts, from which enteroid cultures were established. Enteroid cultures were collected and mixed with pre-chilled Matri gel, plated in 24-well plates and grown in complete medium with growth factors (CMGF+). Enteroids were allowed to differentiate in medium without growth factors for a week before being used for experiments. On the day of experiments, enteroids were washed 3x in complete medium without growth factors (CMGF-) and incubated in CMGF- medium for partial serum starvation. Compositions of CMGF+ and CMGF- media followed exactly those in [31]. For all conditions, the total serum starvation time was 2 hours including each type of treatment.

Whole cell lysates were collected and blotted using antibodies against pMEK, pERK and pAkt. Actin was used as loading control. Each experiment was performed at least 3 times separately and data was shown as mean±SEM. Statistical significance was evaluated using one-way ANOVA, with * indicating $p < 0.05$.

Supplementation of synthetic exogenous PA

Appropriate amount of egg PA dissolved in chloroform (purchased from Avanti Polar Lipids, Inc.) was transferred to a 20-ml glass vial using a Hamilton syringe. Majority of the chloroform was evaporated using N_2 gas and any residual amount of chloroform was eliminated with the glass vial placed under vacuum in the dark overnight. The dried lipid film was re-hydrated with medium and sonicated for 20 minutes in a bath sonicator to generate small unilamellar vesicles for easy incorporation into cells. After sonication, cells were incubated in the medium containing the lipid suspension for 1 hour before harvesting. Proper incorporation of the exogenous PA into the inner leaflet of the PM was validated via immunogold labeling of GFP-PASS (the PA-binding domain) in EM-spatial analysis.

Supporting information

S1 Fig. EM univariate clustering analysis quantifies extent of oligomerization of lipids and EGFR in Caco-2 basolateral PM. EM micrographs of intact basolateral PM of Caco-2 cells ectopically expressing GFP-PASS under control condition (A) or treated with 1μM DCA for 5 minutes (B). GFP-PASS bound to PA on the intact Caco-2 basal PM was immunolabeled with 4.5nm gold nanoparticles conjugated with anti-GFP antibody. (C) Univariate clustering of gold particles labeling various GFP-tagged lipid-binding domains without / with DCA (1μM, 5 minutes) was calculated using K-function analysis. Extent of clustering, $L(r)$-r, was plotted against length scale, r, with the peak value termed as L_{max}. $L(r)$-r values above the 99% confidence interval (99%C.I.) of 1 indicate statistically meaningful clustering, whereas $L(r)$-r values below 99%C.I. indicate uniform distribution. Optimal clustering, L_{max}, (D) and gold labeling (E) of GFP-PASS in Caco-2 cells treated with 1μM of various unconjugated and tauro-conjugated bile acids were quantified using EM-univariate clustering analysis. Optimal clustering (F) and PM binding (G) of GFP-PASS in Caco-2 cells exposed to DCA alone, UDCA alone or combination of both DCA and UDCA were quantified using EM-univariate spatial analysis. Statistical significance between untreated and DCA-treated conditions in all clustering analyses was evaluated using bootstrap tests, with * indicating $p<0.05$. Statistical significance between untreated and DCA-treated conditions in gold labeling was examined using one-way ANOVA, with * indicating $p<0.05$.
(TIF)

S2 Fig. EM-bivariate co-localization analysis quantifies extent of lipid enrichment surrounding EGFR in Caco-2 basal PM. EM micrographs of intact basal PM of Caco-2 cells co-expressing GFP-PASS and EGFR-RFP untreated (A) or treated with 1μM DCA for 5 minutes (B). GFP-PASS was immunolabeled with 6nm gold conjugated to anti-GFP antibody, while EGFR-RFP was immunolabeled with 2nm gold coupled to anti-RFP antibody. (C) Bivariate K-function calculated the co-localization between 6nm and 2nm gold populations on intact Caco-2 basal PM sheets. Extent of co-localization, $L_{biv}(r)$-r, was plotted against length scale, r. $L_{biv}(r)$-r values above the 95%C.I. indicate statistically significant co-localization. Each $L_{biv}(r)$-r curve was then integrated between r values of 10 and 110 to yield integrated L-bivariate, or LBI, to summarize the spatial data. Statistical significance between untreated and DCA-treated conditions in bivariate co-localization analyses was evaluated using bootstrap tests, with * indicating $p<0.05$. (D) Caco-2 cells grown to a monolayer were serum-starved for 2 hours and 30 minutes before treatment of 1μM EGFR specific inhibitor AG1478 for 25 minutes and a subsequent co-incubation with AG1478 and 1μM DCA for 5 minutes. Whole cell lysates were collected and blotted using antibodies against pMEK, pERK, or pAkt. (E) Wild-type CHO cells or CHO cells stably expressing EGFR-GFP were serum-starved for 10 minutes before incubation with 30μM DCA for various time points to ensure total serum starvation time is 30 minutes. Whole cell lysates were collected and blotted against pMEK. Statistical significance was evaluated using one-way ANOVA, with * indicating $p<0.05$.
(TIF)

S3 Fig. DCA stimulates EGFR-MAPK signaling in non-GI cells in similar manner as Caco-2 cells. (A) BHK cells grown to 80–90% confluency were serum-starved for 1 hour before incubation with 30μM DCA for various time points to achieve total serum starvation time of 2 hours. Whole cell lysates were used to blot against pMEK, total MEK, pERK, total ERK, pAkt or total Akt, as well as the loading control actin. (B) BHK cells grown to 80–90% confluency were serum-starved for 1 hour and 55 minutes before incubation with various concentrations of DCA for 5 minutes. Whole cell lysates were used to blot against pMEK, total MEK, pERK,

total ERK, pAkt or total Akt, as well as the loading control actin. (C) BHK cells were serum-starved for 1 hour and 30 minutes before treatment with 1μM AG1478 for 25 minutes and a subsequent co-incubation with AG1478 and 30μM DCA for 5 minutes. Whole cell lysates were used to blot against pMEK, pERK, or pAkt. Statistical significance was evaluated using one-way ANOVA, with * indicating $p<0.05$. (D) EM-univariate clustering experiment was conducted in BHK cells expressing EGFR-GFP without / with 30μM DCA. Intact apical PM sheets of non-polarized BHK cells were attached to EM grids and immunolabeled with 4.5nm gold particles conjugated to anti-GFP antibody. Univariate clustering of the gold particles was quantified using univariate K-function analysis. L_{max} values indicate the extent of oligomerization of EGFR-GFP in apical PM of BHK cells. Statistical significance between untreated and DCA-treated conditions in univariate clustering analyses was evaluated using bootstrap tests, with * indicating $p<0.05$.
(TIF)

Acknowledgments

This work is partially supported by and the National Institutes of Health (NIH: P30 DK056338) and the Cancer Research and Prevention Institute of Texas (CPRIT) (RP130059 and RP170233).

Author Contributions

Conceptualization: Yong Zhou.

Data curation: Hong Liang, Yong Zhou.

Formal analysis: Yong Zhou.

Funding acquisition: Yong Zhou.

Investigation: Yong Zhou.

Methodology: Hong Liang, Mary K. Estes, Huiling Zhang, Guangwei Du, Yong Zhou.

Project administration: Yong Zhou.

Resources: Mary K. Estes, Yong Zhou.

Supervision: Yong Zhou.

Validation: Huiling Zhang, Yong Zhou.

Visualization: Yong Zhou.

Writing – original draft: Yong Zhou.

Writing – review & editing: Mary K. Estes, Guangwei Du, Yong Zhou.

References

1. Hofmann AF, Hagey LR. Key discoveries in bile acid chemistry and biology and their clinical applications: history of the last eight decades. J Lipid Res. 2014; 55(8):1553–95. Epub 2014/05/20. doi: jlr.R049437 [pii] https://doi.org/10.1194/jlr.R049437 PMID: 24838141.
2. Hylemon PB, Zhou H, Pandak WM, Ren S, Gil G, Dent P. Bile acids as regulatory molecules. J Lipid Res. 2009; 50(8):1509–20. Epub 2009/04/07. https://doi.org/10.1194/jlr.R900007-JLR200 PMID: 19346331; PubMed Central PMCID: PMCPMC2724047.
3. Natalini B, Sardella R, Gioiello A, Ianni F, Di Michele A, Marinozzi M. Determination of bile salt critical micellization concentration on the road to drug discovery. J Pharm Biomed Anal. 2014; 87:62–81. Epub 2013/07/23. https://doi.org/10.1016/j.jpba.2013.06.029 PMID: 23870107.

4. Zhou H, Hylemon PB. Bile acids are nutrient signaling hormones. Steroids. 2014; 86:62–8. Epub 2014/05/14. https://doi.org/10.1016/j.steroids.2014.04.016 PMID: 24819989; PubMed Central PMCID: PMCPMC4073476.
5. Nagathihalli NS, Beesetty Y, Lee W, Washington MK, Chen X, Lockhart AC, et al. Novel mechanistic insights into ectodomain shedding of EGFR Ligands Amphiregulin and TGF-alpha: impact on gastrointestinal cancers driven by secondary bile acids. Cancer research. 2014; 74(7):2062–72. Epub 2014/02/13. https://doi.org/10.1158/0008-5472.CAN-13-2329 PMID: 24520077; PubMed Central PMCID: PMCPMC3975694.
6. Ajouz H, Mukherji D, Shamseddine A. Secondary bile acids: an underrecognized cause of colon cancer. World J Surg Oncol. 2014; 12:164. Epub 2014/06/03. https://doi.org/10.1186/1477-7819-12-164 PMID: 24884764; PubMed Central PMCID: PMCPMC4041630.
7. Evans RM, Mangelsdorf DJ. Nuclear Receptors, RXR, and the Big Bang. Cell. 2014; 157(1):255–66. Epub 2014/04/01. https://doi.org/10.1016/j.cell.2014.03.012 PMID: 24679540; PubMed Central PMCID: PMCPMC4029515.
8. Abd Halim KB, Koldso H, Sansom MS. Interactions of the EGFR juxtamembrane domain with PIP2-containing lipid bilayers: Insights from multiscale molecular dynamics simulations. Biochimica et biophysica acta. 2015; 1850(5):1017–25. Epub 2014/09/16. https://doi.org/10.1016/j.bbagen.2014.09.006 PMID: 25219456; PubMed Central PMCID: PMCPMC4547087.
9. Shan Y, Eastwood MP, Zhang X, Kim ET, Arkhipov A, Dror RO, et al. Oncogenic mutations counteract intrinsic disorder in the EGFR kinase and promote receptor dimerization. Cell. 2012; 149(4):860–70. Epub 2012/05/15. https://doi.org/10.1016/j.cell.2012.02.063 S0092-8674(12)00416-3 [pii]. PMID: 22579287.
10. Lu C, Mi LZ, Schurpf T, Walz T, Springer TA. Mechanisms for kinase-mediated dimerization of the epidermal growth factor receptor. J Biol Chem. 2012; 287(45):38244–53. Epub 2012/09/19. https://doi.org/10.1074/jbc.M112.414391 [pii]. PMID: 22988250.
11. Jura N, Endres NF, Engel K, Deindl S, Das R, Lamers MH, et al. Mechanism for activation of the EGF receptor catalytic domain by the juxtamembrane segment. Cell. 2009; 137(7):1293–307. Epub 2009/07/01. https://doi.org/10.1016/j.cell.2009.04.025 PMID: 19563760; PubMed Central PMCID: PMCPMC2814540.
12. Zhou Y, Maxwell KN, Sezgin E, Lu M, Liang H, Hancock JF, et al. Bile acids modulate signaling by functional perturbation of plasma membrane domains. J Biol Chem. 2013; 288(50):35660–70. Epub 2013/10/30. https://doi.org/10.1074/jbc.M113.519116 PMID: 24165125; PubMed Central PMCID: PMCPMC3861618.
13. Mello-Vieira J, Sousa T, Coutinho A, Fedorov A, Lucas SD, Moreira R, et al. Cytotoxic bile acids, but not cytoprotective species, inhibit the ordering effect of cholesterol in model membranes at physiologically active concentrations. Biochim Biophys Acta. 2013; 1828(9):2152–63. Epub 2013/06/12. https://doi.org/10.1016/j.bbamem.2013.05.021 PMID: 23747364.
14. Esteves M, Ferreira MJ, Kozica A, Fernandes AC, Goncalves da Silva A, Saramago B. Interaction of Cytotoxic and Cytoprotective Bile Acids with Model Membranes: Influence of the Membrane Composition. Langmuir. 2015; 31(32):8901–10. Epub 2015/07/29. https://doi.org/10.1021/acs.langmuir.5b01702 PMID: 26218497.
15. Ariotti N, Liang H, Xu Y, Zhang Y, Yonekubo Y, Inder K, et al. Epidermal growth factor receptor activation remodels the plasma membrane lipid environment to induce nanocluster formation. Mol Cell Biol. 2010; 30(15):3795–804. Epub 2010/06/03. doi: MCB.01615-09 [pii] https://doi.org/10.1128/MCB.01615-09 PMID: 20516214; PubMed Central PMCID: PMC2916403.
16. Yeung T, Gilbert GE, Shi J, Silvius J, Kapus A, Grinstein S. Membrane phosphatidylserine regulates surface charge and protein localization. Science. 2008; 319(5860):210–3. Epub 2008/01/12. https://doi.org/10.1126/science.1152066 PMID: 18187657.
17. Zhang F, Wang Z, Lu M, Yonekubo Y, Liang X, Zhang Y, et al. Temporal production of the signaling lipid phosphatidic acid by phospholipase D2 determines the output of extracellular signal-regulated kinase signaling in cancer cells. Mol Cell Biol. 2014; 34(1):84–95. https://doi.org/10.1128/MCB.00987-13 PMID: 24164897; PubMed Central PMCID: PMC3911278.
18. Garcia P, Gupta R, Shah S, Morris AJ, Rudge SA, Scarlata S, et al. The pleckstrin homology domain of phospholipase C-delta 1 binds with high affinity to phosphatidylinositol 4,5-bisphosphate in bilayer membranes. Biochemistry. 1995; 34(49):16228–34. PMID: 8519781.
19. Miao B, Skidan I, Yang J, Lugovskoy A, Reibarkh M, Long K, et al. Small molecule inhibition of phosphatidylinositol-3,4,5-triphosphate (PIP3) binding to pleckstrin homology domains. Proceedings of the National Academy of Sciences of the United States of America. 2010; 107(46):20126–31. Epub 2010/11/03. https://doi.org/10.1073/pnas.1004522107 1004522107 [pii]. PMID: 21041639.

20. Maekawa M, Fairn GD. Complementary probes reveal that phosphatidylserine is required for the proper transbilayer distribution of cholesterol. Journal of cell science. 2015; 128(7):1422–33. https://doi.org/10.1242/jcs.164715 PMID: 25663704.

21. Garry FB, Fettman MJ, Curtis CR, Smith JA. Serum bile acid concentrations in dairy cattle with hepatic lipidosis. J Vet Intern Med. 1994; 8(6):432–8. Epub 1994/11/01. PMID: 7884730.

22. Zhou Y, Prakash P, Liang H, Cho KJ, Gorfe AA, Hancock JF. Lipid-Sorting Specificity Encoded in K-Ras Membrane Anchor Regulates Signal Output. Cell. 2017; 168(1–2):239–51 e16. Epub 2017/01/04. https://doi.org/10.1016/j.cell.2016.11.059 PMID: 28041850; PubMed Central PMCID: PMCPMC5653213.

23. Zhou Y, Wong CO, Cho KJ, van der Hoeven D, Liang H, Thakur DP, et al. SIGNAL TRANSDUCTION. Membrane potential modulates plasma membrane phospholipid dynamics and K-Ras signaling. Science. 2015; 349(6250):873–6. Epub 2015/08/22. https://doi.org/10.1126/science.aaa5619 349/6250/873 [pii]. PMID: 26293964.

24. Jean-Louis S, Akare S, Ali MA, Mash EA Jr., Meuillet E, Martinez JD. Deoxycholic acid induces intracellular signaling through membrane perturbations. J Biol Chem. 2006; 281(21):14948–60. Epub 2006/03/21. doi: M506710200 [pii] https://doi.org/10.1074/jbc.M506710200 PMID: 16547009.

25. Zhao C, Du G, Skowronek K, Frohman MA, Bar-Sagi D. Phospholipase D2-generated phosphatidic acid couples EGFR stimulation to Ras activation by Sos. Nat Cell Biol. 2007; 9(6):706–12. Epub 2007/05/09. doi: ncb1594 [pii] https://doi.org/10.1038/ncb1594 PMID: 17486115.

26. Qiao L, Studer E, Leach K, McKinstry R, Gupta S, Decker R, et al. Deoxycholic acid (DCA) causes ligand-independent activation of epidermal growth factor receptor (EGFR) and FAS receptor in primary hepatocytes: inhibition of EGFR/mitogen-activated protein kinase-signaling module enhances DCA-induced apoptosis. Mol Biol Cell. 2001; 12(9):2629–45. Epub 2001/09/13. https://doi.org/10.1091/mbc.12.9.2629 PMID: 11553704.

27. Rao YP, Studer EJ, Stravitz RT, Gupta S, Qiao L, Dent P, et al. Activation of the Raf-1/MEK/ERK cascade by bile acids occurs via the epidermal growth factor receptor in primary rat hepatocytes. Hepatology. 2002; 35(2):307–14. Epub 2002/02/05. doi: S0270913902252921 [pii] https://doi.org/10.1053/jhep.2002.31104 PMID: 11826403.

28. Chen X, Resh MD. Cholesterol depletion from the plasma membrane triggers ligand-independent activation of the epidermal growth factor receptor. J Biol Chem. 2002; 277(51):49631–7. Epub 2002/10/25. https://doi.org/10.1074/jbc.M208327200 PMID: 12397069.

29. Wilken JA, Baron AT, Maihle NJ. The epidermal growth factor receptor conundrum. Cancer. 2011; 117(11):2358–60. Epub 2011/06/01. https://doi.org/10.1002/cncr.25805 PMID: 24048781.

30. Saxena K, Blutt SE, Ettayebi K, Zeng XL, Broughman JR, Crawford SE, et al. Human Intestinal Enteroids: a New Model To Study Human Rotavirus Infection, Host Restriction, and Pathophysiology. J Virol. 2016; 90(1):43–56. Epub 2015/10/09. https://doi.org/10.1128/JVI.01930-15 PMID: 26446608; PubMed Central PMCID: PMCPMC4702582.

31. Ettayebi K, Crawford SE, Murakami K, Broughman JR, Karandikar U, Tenge VR, et al. Replication of human noroviruses in stem cell-derived human enteroids. Science. 2016; 353(6306):1387–93. Epub 2016/08/27. https://doi.org/10.1126/science.aaf5211 PMID: 27562956; PubMed Central PMCID: PMCPMC5305121.

32. Zou WY, Blutt SE, Crawford SE, Ettayebi K, Zeng XL, Saxena K, et al. Human Intestinal Enteroids: New Models to Study Gastrointestinal Virus Infections. Methods Mol Biol. 2017. Epub 2017/04/01. https://doi.org/10.1007/7651_2017_1 PMID: 28361480.

33. McLaughlin S, Smith SO, Hayman MJ, Murray D. An electrostatic engine model for autoinhibition and activation of the epidermal growth factor receptor (EGFR/ErbB) family. J Gen Physiol. 2005; 126(1):41–53. Epub 2005/06/16. https://doi.org/10.1085/jgp.200509274 PMID: 15955874; PubMed Central PMCID: PMCPMC2266615.

34. Orr G, Hu D, Ozcelik S, Opresko LK, Wiley HS, Colson SD. Cholesterol dictates the freedom of EGF receptors and HER2 in the plane of the membrane. Biophys J. 2005; 89(2):1362–73. Epub 2005/05/24. https://doi.org/10.1529/biophysj.104.056192 PMID: 15908575; PubMed Central PMCID: PMCPMC1366621.

35. Fuentes NR, Mlih M, Barhoumi R, Fan YY, Hardin P, Steele TJ, et al. Long-Chain n-3 Fatty Acids Attenuate Oncogenic KRas-Driven Proliferation by Altering Plasma Membrane Nanoscale Proteolipid Composition. Cancer research. 2018; 78(14):3899–912. Epub 2018/05/18. https://doi.org/10.1158/0008-5472.CAN-18-0324 PMID: 29769200; PubMed Central PMCID: PMCPMC6050089.

36. Wilson SR, Nelson AM, Batia L, Morita T, Estandian D, Owens DM, et al. The ion channel TRPA1 is required for chronic itch. The Journal of neuroscience: the official journal of the Society for Neuroscience. 2013; 33(22):9283–94. https://doi.org/10.1523/JNEUROSCI.5318-12.2013 PMID: 23719797; PubMed Central PMCID: PMC3752436.

37. Taberner FJ, Fernandez-Ballester G, Fernandez-Carvajal A, Ferrer-Montiel A. TRP channels interaction with lipids and its implications in disease. Biochim Biophys Acta. 2015; 1848(9):1818–27. https://doi.org/10.1016/j.bbamem.2015.03.022 PMID: 25838124.

38. Lieu T, Jayaweera G, Zhao P, Poole DP, Jensen D, Grace M, et al. The bile acid receptor TGR5 activates the TRPA1 channel to induce itch in mice. Gastroenterology. 2014; 147(6):1417–28. https://doi.org/10.1053/j.gastro.2014.08.042 PMID: 25194674; PubMed Central PMCID: PMC4821165.

39. Diggle PJ, Mateu J, Clough HE. A comparison between parametric and non-parametric approaches to the analysis of replicated spatial point patterns. Adv in Appl Probab. 2000; 32(2):331–43.